



Neuromuscular basis of *Drosophila* larval rolling escape behavior

Patricia C. Cooney^{a,b,1}, Patricia C. Cooney^{a,b,1}, Yuhan Huang^{c,d,1}, Wenze Li^{e,f}, Dulanjana M. Perera^g, Richard Hormigo^a, Tanya Tabachnik^a, Isuru S. Godage^{g,h,j}, Elizabeth M. C. Hillman^{e,j,k}, Wesley B. Grueber^{a,b,l,2}, and Aref A. Zarin^{c,d,2}

Edited by Alex Kolodkin, Johns Hopkins University School of Medicine, Baltimore, MD; received March 3, 2023; accepted October 6, 2023

When threatened by dangerous or harmful stimuli, animals engage in diverse forms of rapid escape behaviors. In Drosophila larvae, one type of escape response involves C-shaped bending and lateral rolling followed by rapid forward crawling. The sensory circuitry that promotes larval escape has been extensively characterized; however, the motor programs underlying rolling are unknown. Here, we characterize the neuromuscular basis of rolling escape behavior. We used high-speed, volumetric, Swept Confocally Aligned Planar Excitation (SCAPE) microscopy to image muscle activity during larval rolling. Unlike sequential peristaltic muscle contractions that progress from segment to segment during forward and backward crawling, muscle activity progresses circumferentially during bending and rolling escape behavior. We propose that progression of muscular contraction around the larva's circumference results in a transient misalignment between weight and the ground support forces, which generates a torque that induces stabilizing body rotation. Therefore, successive cycles of slight misalignment followed by reactive aligning rotation lead to continuous rolling motion. Supporting our biomechanical model, we found that disrupting the activity of muscle groups undergoing circumferential contraction progression leads to rolling defects. We use EM connectome data to identify premotor to motor connectivity patterns that could drive rolling behavior and perform neural silencing approaches to demonstrate the crucial role of a group of glutamatergic premotor neurons in rolling. Our data reveal body-wide muscle activity patterns and putative premotor circuit organization for execution of the rolling escape response.

rolling escape behavior | premotor-motor-muscle connectome | motor circuits | nociception | Drosophila larvae

Early in the evolution of animals, nervous systems specialized to permit locomotion (1). While locomotion supports multiple aspects of evolutionary success (e.g., allocating resources, finding mates), one of the most critical of these is escape: the transformation of sensory input into motor output to avoid imminent danger (2-4). Escape behaviors are rapid and stereotyped, yet must be flexible enough to allow animals to evade multiple sources of harm and readjust when danger subsides (3, 5, 6). Escape behaviors across species often differ fundamentally from exploratory locomotion (3, 7–11). This specificity suggests that dedicated neural circuits or unique activity patterns within shared locomotor circuits are employed during escape. While many studies have investigated how sensory input promotes escape (2, 3, 6, 8, 9, 12–16), the neuromuscular activity that generates escape movements has been characterized in few model organisms (8, 12, 17, 18). Furthermore, the model systems in which escape movement generation has been studied have yielded limited understanding of how the sensory circuits that promote escape drive motor circuits. By characterizing escape motor circuits in the *Drosophila* model, with its well-studied sensory system and nearly complete connectome, we aim to understand how sensory input is transformed into motor output during escape.

The Drosophila larval body consists of twelve segments, with abdominal segments containing up to 60 different muscles (19). Forward crawling consists of sequential segmental contractions that propagate from posterior to anterior segments and engages all muscles (19-21). Upon experiencing harmful mechanical stimuli or heat, larvae initiate a nocifensive escape consisting of C-shaped bending, rolling, and rapid forward crawling (22). Rolling causes fast lateral motion—which is faster than escape crawling alone and can dislodge attacking parasitoid wasps (23, 24). This behavior is initiated by activity of class IV (cIV) dendritic arborization neurons, polymodal nociceptors that tile the body wall (23, 25). Several downstream partners of cIV neurons have been identified and reconstructed using serial transmission electron microscopy (26–30). Activation of any of several interneurons that are downstream of cIV neurons is sufficient to evoke a rolling escape response (26, 27, 30), but how these interneurons drive downstream motor activity patterns remains poorly characterized.

Significance

To escape from dangerous stimuli, animals execute escape behaviors that are fundamentally different from normal locomotion. The rolling escape behavior of *Drosophila* larvae consists of C-shaped bending and rolling. However, the muscle contraction patterns that lead to rolling are poorly understood. We find that following the initial body bending, muscles contract in a circumferential wave around the larva as they enter the bend, maintaining unidirectional rolling that resembles a cylinder rolling on a surface. We study the structure of motor circuits for rolling, inhibit different motor neurons to determine which muscles are essential for rolling, and propose circuit and biomechanical models for roll generation. Our findings provide insights into how motor circuits produce diverse motor behaviors.

Author contributions: P.C.C., W.B.G., and A.A.Z. designed research; P.C.C., Y.H., W.L., and A.A.Z. performed research; P.C.C., W.L., D.M.P., R.H., T.T., I.S.G., E.M.C.H., W.B.G., and A.A.Z. contributed new reagents/analytic tools; P.C.C., Y.H., W.L., E.M.C.H., and A.A.Z. analyzed data; P.C.C., I.S.G., W.B.G., and A.A.Z. wrote the paper.

Competing interest statement: SCAPE intellectual property is licensed to Leica Microsystems and Applied Scientific Instrumentation (ASI). EMCH and WL could benefit financially from the sale of resulting commercial systems.

This article is a PNAS Direct Submission.

Copyright © 2023 the Author(s). Published by PNAS. This open access article is distributed under Creative Commons Attribution-NonCommercial-NoDerivatives License 4.0 (CC BY-NC-ND).

¹P.C.C. and Y.H. contributed equally to this work.

²To whom correspondence may be addressed. Email: azarin@bio.tamu.edu or wg2135@columbia.edu.

This article contains supporting information online at https://www.pnas.org/lookup/suppl/doi:10.1073/pnas. 2303641120/-/DCSupplemental.

Published December 14, 2023.

Despite progress in understanding nociceptive circuitry, characterizing neural and muscular activity during escape behavior presents challenges. In contrast to crawling, rolling behavior is asymmetric, with larvae rolling laterally in one direction. However, both the larval body and central nervous system (CNS) are symmetric on either side of the dorsal and ventral midlines. The hemisegment unit is important to consider during rolling behavior since the bilaterally symmetric neural and muscle activity that occurs during crawling must be broken during rolling, setting up a fundamental difference between these two behaviors.

In this study, we examine the muscle activity and motor circuits responsible for escape bending and rolling using a combination of high-speed 3D imaging of fluorescent calcium indicators expressed in muscles, functional manipulations of motor circuits, and connectomics approaches. We compare our findings to the motor activity that drives crawling to identify what features of peristaltic locomotor drive are preserved in escape and what motor features are unique to rolling escape locomotion. Both behaviors involve sequential motor activity and antagonistic drive of distinct muscle groups, but our results highlight fundamental differences in the motor patterns. In particular, muscle contractions progress circumferentially around the larva during rolling, in contrast to the anteroposterior progression of muscle contractions during crawling. These data provide a foundational view of motor activity during larval rolling, narrowing in on a full sensory to motor understanding of an escape behavior.

Results

Muscle Activity Patterns in Rolling Escape Behavior. Drosophila larval rolling escape is comprised of C-shaped bending followed by lateral rolling (22). Rolling can be triggered experimentally by activation of nociceptive sensory neurons or by central neurons including the Goro command neuron (26). We confirmed that in response to optogenetic activation of Goro or a global heat nociceptive stimulus, larvae engage in bending and rolling behavior. We found that larvae can bend to the left or right, and, independent of bend direction, may roll in a clockwise or counterclockwise direction (Fig. 1A and Movie S1). Thus, upon optogenetic activation of nociceptive circuitry, larvae can engage four distinct, yet related, escape motor patterns.

Circuitry triggering the rolling escape behavior is well studied in Drosophila larvae, but how circuitry converges on premotor and motor systems is not known. We therefore sought to determine the muscle activity that underlies the escape rolling motor pattern. We imaged larvae using Swept Confocally Aligned Planar Excitation (SCAPE) microscopy, a volumetric imaging technique that permits high-speed, high-resolution, 3D imaging of behaving animals (31–38). We induced rolling using Goro activation in larvae expressing mCherry and GCaMP6f in all body wall muscles. We resolved activity of individual muscles along the entire length of the larva and approximately half of the body thickness, at 10 volumes per second (Fig. 1B and SI Appendix, Fig. S1 A and B and Movie S2). Simultaneously acquired, static mCherry signals were used to ratiometrically correct GCaMP signals to remove artifacts relating to movement. We predicted that as GCaMP6f/mCherry ratios increased, muscle length would decrease, reflecting muscle contraction upon activation. Indeed, these two measurements showed an inverse relationship, suggesting that GCaMP6f/mCherry ratios can be used as an indicator of muscle contraction (SI Appendix, Fig. S1C). We focused the bulk of our analysis on muscles in mid-segments A2-A4 since activity in these showed the greatest dynamic range (SI Appendix, Fig. S1 C). We analyzed roughly 19 muscles per hemisegment in A2-A4 across multiple roll events, and in A1 and A5 during two roll events, totaling over 520 muscle measurements.

SCAPE recordings revealed that muscles are most active along the bent side of the larva, consistent with a role for asymmetric muscle contractions in C-shaped bending (Movie S3 and Fig. 1B). Ratiometric calcium signals for many muscles tended to decrease as muscles moved out of the bend (Movie S3 and SI Appendix, Figs. S2 A–D and S3 A–C) and to increase as muscles rotated into the bend (Movie S3 and SI Appendix, Fig. S2E). To contrast escape rolling and crawling at the level of individual muscles, we compared SCAPE imaging data collected during rolling to previously acquired confocal data on muscle activity during crawling (21) (Fig. 1 B and C and SI Appendix, Fig. S3 D and E). As expected, measurements of muscle peak calcium activity during crawling revealed a delay between muscle contraction in neighboring segments during peristalsis (Fig. 1 C and D). By contrast, during rolling, segmentally homologous muscles showed synchronous contractions, primarily on the side of the larva entering the bend. Also, in contrast to peristalsis, sequential muscle activity traveled around the circumference of the larva during rolling (Fig. 1 B, E, and F and SI Appendix, Figs. S4 and S3 *D* and *E*). Notably, we found that while dorsal (D) and ventral (V) longitudinal and oblique muscles demonstrated significantly greater activity along the bent side than the stretched side of the larva, lateral transverse (LTs) and ventral acute (VAs) muscles show a different activation pattern. Specifically, VA muscles show only a moderate decrease in activity between the bent and stretched sides of the larva. LT muscles show heterogeneous activity patterns, where ~60% demonstrate roughly equivalent activity in each phase of the roll and ~40% demonstrate increasing activity as they approach the stretched side of the larva (Fig. 2 *A*–*C*). These primary features of muscle activity are consistent across segments A1-A5, though LT muscles are more likely to increase activity as they approach the stretched side of the larva in midsegments A2-A4 than in distal segments A1 and A5, and VA muscles show significant decreases in activity in A1 and A5, analogous to longitudinal muscles (SI Appendix, Fig. S3 B-D). Therefore, LT and VA muscles do not follow the typical circumferential wave of activity seen in other body wall muscles.

Altogether, these data demonstrate crucial distinctions between motor patterns during rolling and crawling: 1) Muscle activity during rolling is synchronous across segments but is intersegmentally asynchronous during crawling; 2) muscle activity is left-right asymmetric during rolling but is left-right symmetric during crawling; 3) rolling involves progression of muscle contractions around the circumference of the larva, while crawling involves progression of muscle contractions along the anteroposterior axis. As an important exception to (2) above, we predict that as larvae roll, there are short periods of bilateral synchronicity (momentary left-right hemisegmental symmetry), during which homologous muscles flanking the dorsal (i.e., left and right DLs) or ventral midline (i.e., left and right VOs) enter the bend and co-contract. However, rolling and crawling are similar in that the within-segment muscle activity patterns both demonstrate opposing functions of longitudinally spanning versus transverse-spanning (LT and VA) muscles.

The Biomechanics of Larval Rolling Motion. So far, we have shown that activation of the Goro command neurons result in propagation of muscle contraction around the circumference of the larvae. But how does the circumferential progression of muscle contraction lead to the rolling motion that translates the larval body on the surface? To address this question and further elucidate the biomechanics of larval rolling, we propose the following mechanics model for inward (counterclockwise with respect to the head) (Fig. 3 A–E and Movie S4) and outward (clockwise with respect to the head) (Fig. 3 F–I and Movie S4) rolling motions.

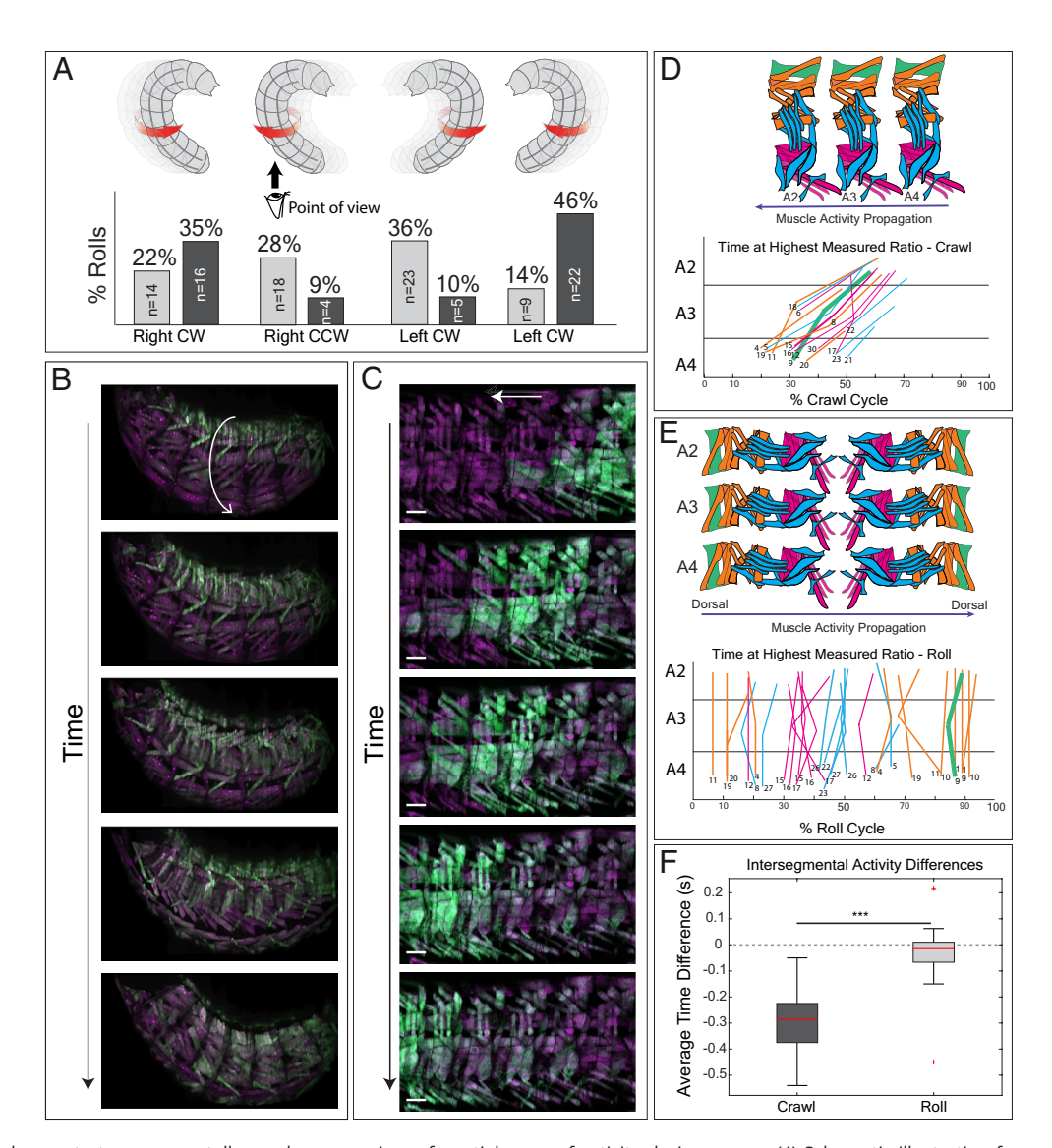


Fig. 1. Muscles demonstrate a segmentally synchronous, circumferential wave of activity during escape (A) Schematic illustrating four patterns of escape observed, based on combination of which side larva bends toward (left or right) and which direction the larva rotates (clockwise or counterclockwise). Translation direction is determined by direction of rotation. Histogram shows frequency of escape patterns observed in response to sustained optogenetic Goro activation (light gray, n = 64 rolls) or in response to global heat + vibration stimulus (dark gray, n = 47 rolls). (B) Maximum intensity projections (MIPs) of SCAPE volumes from a single roll bout, showing the same muscle appearing in focal plane simultaneously across segments (Green and Magenta represent GCaMP and mCherry signals, respectively). Muscle GCaMP increased primarily on the bent side of the larva. The arrow indicates the direction of larval rotation. (C) Confocal dual-color stills from single crawl bout in larva, demonstrating increase in GCaMP brightness from posterior to anterior muscles during single crawl bout. (D) Schematic of muscle arrangement in three neighboring hemisegments, color coded by muscle groups. The blue arrow indicates posterior-to-anterior propagation of muscle activity. Peak ratiometric muscle fluorescence times during single crawl bout across three segments with the muscle number at the bottom of the line. During forward crawling, muscles of segment A4 reach peak activity before A3, and muscles of segment A3 reach peak activity before A2 segment, demonstrating the propagation of peristaltic contraction from posterior to anterior segments. Representative homologous muscle across hemisegments and peak activity lines in green for clarity of segmental propagation of activity during crawling. (E) Three-segment schematic of hemisegments, color coded by muscle groups, as established in Landgraf et al. (2003). The blue arrow indicates circumferential propagation of muscle activity. Highest observed ratiometric muscle fluorescence times during single roll cycle with SCAPE across segments A2-A4 with the muscle number at the bottom of each line. The same muscle types across segment A2 to A4 simultaneously reach their peak activity. Muscles are color-coded according to panel D, demonstrating dorsal to ventral to dorsal (circumferential) propagation of muscle contraction. Representative homologous muscle across segments and peak activity lines in green indicate an example of segmental synchrony of activity during rolling. (F) Comparison between time difference of muscles in segments A2-A4 for forward crawling versus rolling (crawl: n = 2crawls, 2 larvae, 86 muscles; roll: n = 4 rolls, 3 larvae, 372 muscles). Negative values indicate that muscles in the adjacent posterior segment are active before muscles in the adjacent anterior and "0" indicates synchronous contraction. Mann-Whitney U tests were performed between intersegmental roll lag values and intersegmental crawl lag values. P values are indicated as ***P < 0.001 [Scale bars, 100 μm (B) and 50 μm (C)].

Here, we describe a discrete and infinitesimal propagation of the bending plane and the subsequent force and moment imbalance to illustrate the larval rolling locomotion. A larva with a flat pose lying on a surface experiences two distinct forces: its weight (W = mg,where m is the mass of the body and g is the gravitational acceleration) and the distributed ground reaction force (F_R) from the contact points between the body and ground (Fig. 3A). To achieve initial bending and form a C-shaped body conformation, the larva unilaterally

activates (contracts) its ventrolateral muscles (VLs) on the right side (Fig. 3B). Next, the muscle groups located above the VLs become activated (i.e., clockwise propagation of muscular contraction with respect to the head), causing the head and tail of the larva to undergo an infinitesimal move upward (Fig. 3C). According to our model, an upward displacement would generate a force imbalance, causing the distributed ground reaction force to act solely on the contact points near the center of the body (Fig. 3C) as the friction between the larva

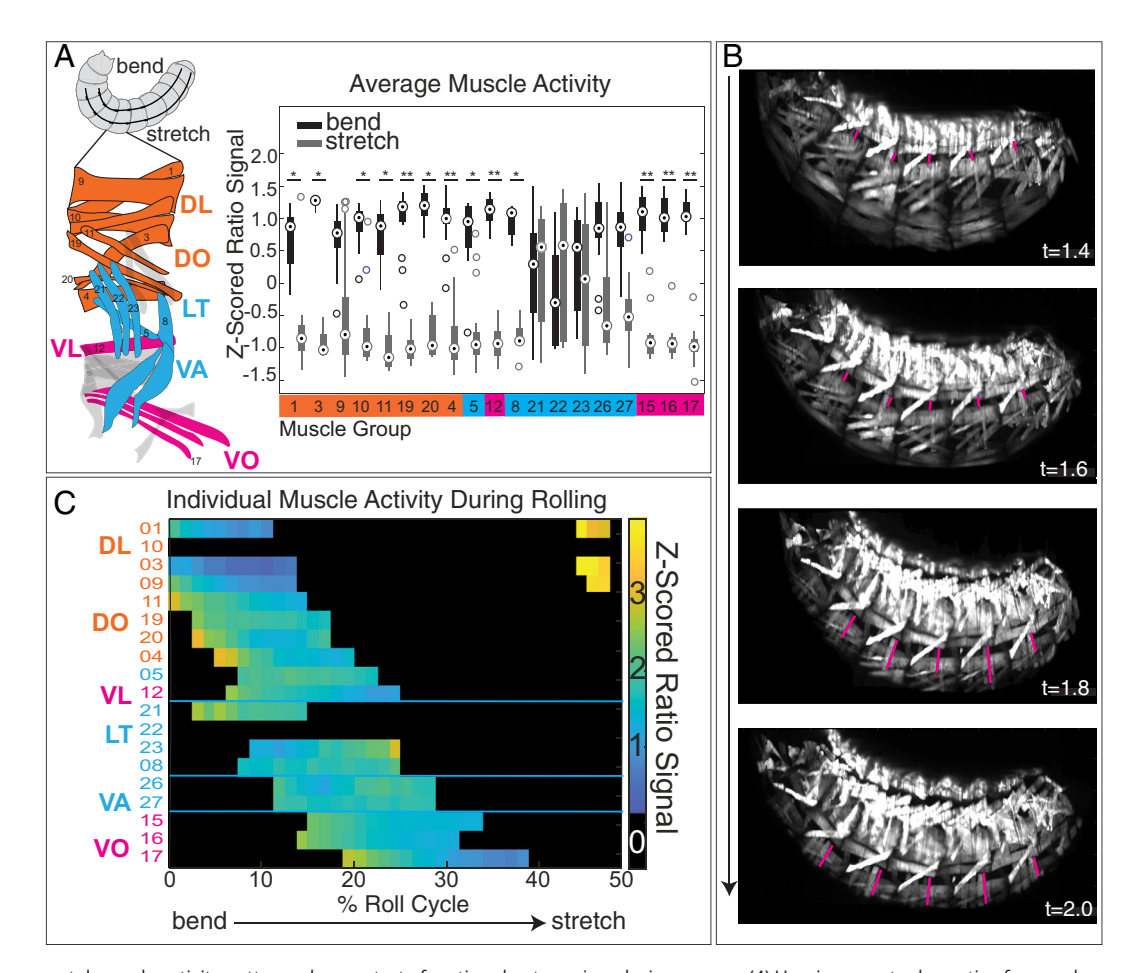


Fig. 2. Intrasegmental muscle activity patterns demonstrate functional antagonism during escape. (A) Hemisegment schematic of example measured muscles color-coded according to Landgraf et al. (2003) (*Left*). Boxplot showing the mean z-scored ratio signal for individual muscles from frames when muscles were along the bent side of the larva (black) vs. along the stretched side of the larva (gray) (*Right*). Data are grouped and color-coded along the x-axis according to dorsoventral order and similarity of activity patterns. Orange muscles and magenta muscles (dorsal longitudinal, DL; dorsal oblique, DO; ventral longitudinal, VL; ventral oblique, VO) show an increased ratio signal along the bent side of the larva, while cyan (lateral transverse, LT) muscles show on average equivalent ratiometric signal on bent and stretched sides. Cyan (ventral acute, VA) muscles show elevated activity on the bent side, but the difference between activity in bent and stretched sides is insignificant (*n* = 3 rolls, 3 larvae, 280 muscles). See *SI Appendix*, Fig. S2*F* for frequency of equivalent vs. increasing LT and VA activity patterns. (*B*) Examples of ratiometric GCaMP/mCherry SCAPE data shown as MIPs for a sequence of time-points. Magenta lines highlight lateral transverse (LT) muscles, demonstrating a low ratio signal while rotating out of the bend and increased ratio signal while rotating toward the stretched side of the larva. (*C*) Heatmap of z-scored ratio signal across individually measured muscles in one example hemisegment, organized from dorsal (top row) to ventral (bottom row). LT ratiometric traces show mixed activity patterns (23 increases activity while 21 and 8 show roughly equivalent activity as they rotate toward the bend), an activity pattern different from other muscles. VA ratiometric traces show roughly equivalent activity the roll. Color bar to the right of shows the range of z-scored ratio signal values. Black indicates frames when muscles were out of the FOV and not measured. (Scale bars, 100 μm.)

cuticle and surface (F_f) prevents the body from slipping. Consequently, the reaction force no longer aligns with the body weight (Fig. 3D), resulting in a moment of imbalance, τ_m , which induces a fall back to the ground and counterclockwise rotation (with respect to the head) to restore the distributed contact (Fig. 3E). Therefore, during this process, the clockwise progression of muscle contraction causes the larva's body to undergo a counterclockwise rotation, leading to inward translation of the entire soft body (Fig. 3 B–E). We propose that continuous and successive cycles of imbalance followed by reactive rotation leads to continuous rolling motion. The actual body translation of the larva rotating on the surface results from differential friction reaction forces between the larva's cuticle (outer coverings) and the contact surface, following the same laws of physics applicable to a tire rotating on a surface. See Movie S4 for animated version of this model.

On the other hand, if after the initial C-shaped body conformation (Fig. 3F), contraction of the muscle groups located below the VLs (i.e., counterclockwise propagation of muscular contraction with respect to the head) would infinitesimally move the larva's mid-body upward while its head and tail are still in touch

with the surface (Fig. 3G). Based on our proposed model, an upward movement would generate a force imbalance that causes the distributed force to act solely on the contact points near the head and tail (Fig. 3H). Consequently, the reaction force no longer aligns with the body weight, resulting in a moment of imbalance, τ_m , which triggers a fall back of the mid-body to the ground, followed by clockwise rotation of the entire body to rectify the static imbalance and restore stability via distributed contact (Fig. 3I). Therefore, during this process, the counterclockwise progression of muscle contraction produces clockwise rotation, leading to outward translation of the entire soft body (Fig. 3I). Based on this model, successive continuous cycles of imbalance followed by reactive rotation lead to continuous rolling motion. See Movie S4 for animated version of this model.

Our biomechanical models of clockwise and counterclockwise rolling were adopted from two recent robotics studies by Arachchige et al. (39, 40), who extensively modeled the kinematics and physics of rolling and constructed soft robotic snakes (SRS) performing inward and outward rolling motions (*SI Appendix*, Fig. S5 *A* and *B* and Movie S5) identical to those of *Drosophila* larvae. The trajectories

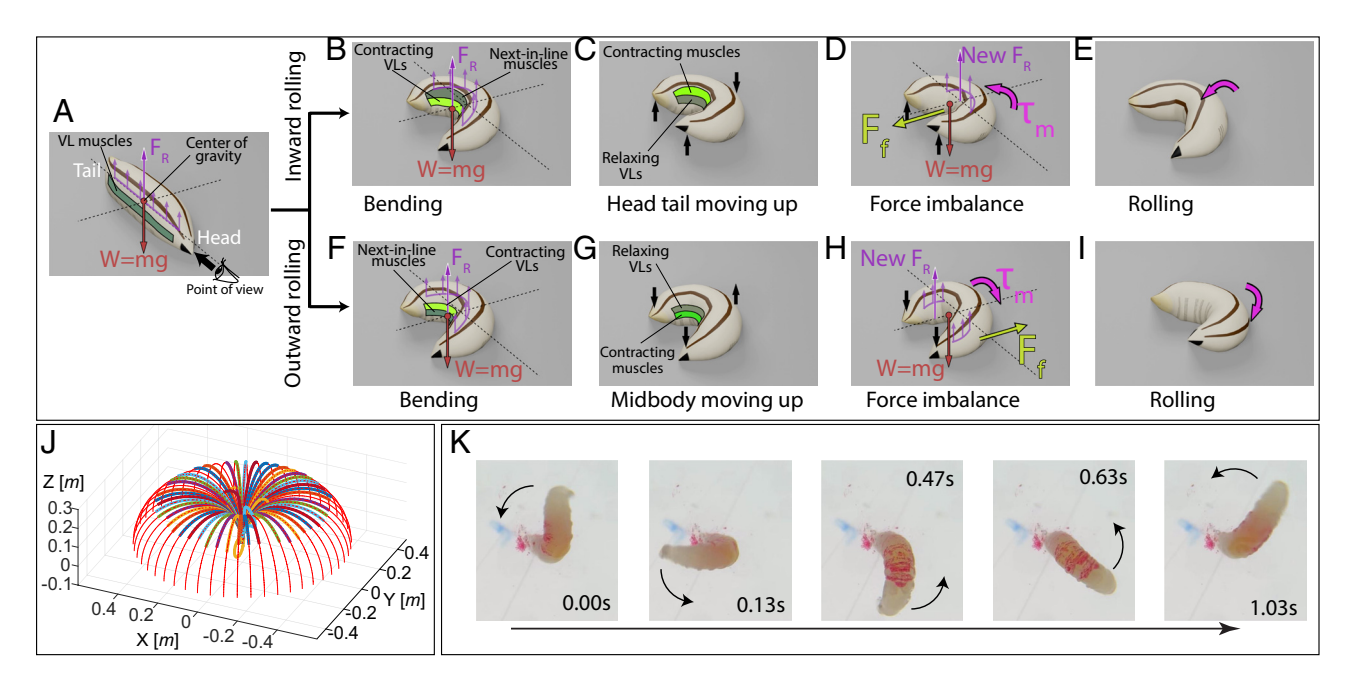


Fig. 3. 3D model of larva demonstrating the biomechanics of rolling. Larval rolling is driven by the discrete and infinitesimal propagation of the bending plane and the subsequent force and moment imbalance. There are two types of rolling: Inward rolling (A-E) is when the larva rolls toward the bend (counterclockwise when viewing from the head), and outward rolling (A and F-I) is when the larva rolls away from the bend (clockwise when viewing from the head). (A) Model of a larva lying flat on a surface without bending. The weight (W = mg) is balanced by and aligned with the sum of ground reaction forces (F_R) that are evenly distributed at contact points between the larval body and the surface. m is the mass of the object and g gravitational acceleration. (B-E) Steps specific to inward rolling (counterclockwise with respect to the head). (B) The larva bends into a C-shape by contracting its ventrolateral muscles (VLs). This causes a shift of its center of gravity (CoG) toward the bend and away from the anteroposterior axis of the body, but W is still aligned with the sum of ground reaction force (FR). After initial bending, the muscles above VLs are the next in line to be activated. (C) The muscles above the VLs are activated, causing the head and tail to slightly move upward, leading to a slight shift of the bending plane. (D) Because the head and tail are no longer touching the ground, the point of application of the sum of ground reaction forces moves to the middle body segments that are in contact with the ground. The concentrated sum of reaction forces to the mid-segments no longer aligns with its body weight. The imbalance of forces causes a moment (torque), τ_{m} , which induces counterclockwise rolling. While this torque makes the larva tend to slip away from the bend, a static friction (F_i) is applied to the larva, oriented toward the bend to prevent slipping. (E) The larva rotates counterclockwise (toward the bend opening) as it falls back to the surface. (F-I) Steps specific to outward rolling (clockwise with respect to the head). (F) After initial bending, the muscles below VLs are the next to be activated. (G) The muscles below VLs are activated, causing a downward movement of the head and tail while the mid-segments of the body are slightly lifted. (H) The change of contact points causes the sum of F_R to move away from the middle segments toward the bend, no longer aligning with weight. The static friction F_f in this case is oriented away from the bend. (I) The imbalance of forces causes a moment $\tau_{\rm m}$ that induces clockwise rolling as the larva falls back to the surface. For clarity and ease of understanding, the upward movements are exaggerated in panels C and G of this Figure and the related animations (Movie S4). In reality, we'd expect any upward displacement to be very small given the soft nature of the larva. (f) Spatial trajectories of a soft robotic snake (SRS) attempting to perform rolling in the absence of a solid surface generate a rotational motion that is reminiscent of a semicircular windmill blade rotating around the central post. We refer to this motion as "windmill blade model" (adopted from Arachchige et al. (39, 40) with permission). (K) Experimental validation of the windmill blade model using Drosophila larva. A series of still images demonstrates the "windmill blade" motion of a larva oriented vertically with its tail stuck in an agarose gel, showing the same spatial trajectory as the SRS in (J). The screenshots are taken at 0°, 90°, 180°, 225°, and 315° positions during a full 360° windmill blade roll. The larva is rolling counterclockwise. The dorsal side of the larva is labeled with a red marker to show the rotation of the body. At 0° position, the red mark is invisible but becomes fully visible at 180° position and becomes invisible again as the larva complete the roll.

for these rolling motions were generated from circumferential progression of bending of the entire body, similar to what we observe in larval rolling. Once the SRS is provided with the commands to generate circumferential progression of bending while the SRS is on the ground, it engages in rolling locomotion—both clockwise and counterclockwise directions (the authors termed these gaits are inward and outward rolling) (SI Appendix, Fig. S5 A and B and Movie S5) (39, 40).

To further determine the impact of friction reaction forces between SRS skin and the contact surface, Arachchige et al. formulated the mathematical basis of spatial trajectories for an SRS attempting to perform rolling in a three-dimensional (3D) space with no solid surface to interact with its skin. In this simulation, the SRS is anchored to the ground from one end while the rest of its body is up in the air. Based on their formulation, following the initial bending, the SRS forms a C-shaped structure with one end attached to the surface and the other end up in air. Subsequently, while circumferential progression of contraction occurs, the SRS maintains its C-shape and its free end undergoes rotation (circular movement) around the end touching the surface, resembling a semicircular windmill blade rotating around the central post

(Fig. 3J) (39, 40). This simulated 3D motion (hereafter referred to as windmill blade movement) indicated that for circumferentially propagating contraction to be transformed into a rolling behavior, the SRS needs to interact with a surface, thereby generating the friction reaction forces necessary for rolling. We used Drosophila larvae to experimentally test and validate the windmill blade movement. We inserted larval posterior segments (A7–A9) into a nick made on an agarose pad, positioning the larva perpendicular to the surface with its head and the rest of the segments free to move in a 3D space (i.e., air) (Fig. 3K and Movie S6). Upon Goro activation, the larva formed a semicircular C-shaped structure and continuously rotated around its point of contact with agarose (Fig. 3K and Movie S6). In this setup, if the larva exits the nick and acquires a flat pose lying on the surface, the windmill blade motion is converted back to normal larval rolling. In another experiment, we optogenetically activated Goro and first allowed the larva to roll on the surface and then lifted the animal off the surface while rolling. Once the larva was suspended in the air, it began producing windmill blade movement (Movie S6). These data not only corroborate the windmill blade model but also reveal the role of surface friction in rolling.

The muscle activity we captured by SCAPE microscopy, though primarily a circumferential progressing muscular contraction, also consisted of LT and VA muscle activity that sustained or increased counter to bend propagation. We propose that these muscles contribute to the mechanics of rolling in two ways. First, it is likely that optimal rigidity must be maintained for the efficient rolling of soft-bodied animals. If so, the prolonged activity windows of the larvae's LT and VA muscles could be involved in adjusting and maintaining internal body pressure, thus ensuring the optimal rigidity necessary for the larval soft body to function as a muscular hydrostat, similar to the hydrostatic skeletons observed in animal tongues and cephalopod arms (41). Second, transverse (LT) muscle activity might provide a pulling force that aids in generating body rotation. Although our biomechanical model achieves bending and rolling with strictly longitudinal contractile forces, it does not rule out the possible contribution of other muscles with distinct orientations to larval rolling. We test the functional contributions of distinct muscles in the following section.

The Activities of a Variety of Dorsal, Lateral, and Ventral Muscles Is Required for Rolling. Our SCAPE imaging and biomechanical model suggests that a circumferential propagation of muscular contraction underlies the torque required for larval rolling. However, the muscles and MN types that are essential for rolling are unknown. Many larval body muscles are co-innervated by type Is and a single type Ib excitatory MNs (Fig. 4A). Each type Is MN innervates multiple target muscles, has a phasic firing pattern, and makes smaller synaptic boutons in neuromuscular junctions (NMJs). Type Ib MNs, by contrast, typically innervate one muscle, have a tonic firing pattern, and establish larger synaptic boutons in their NMJs (42, 43). There are two phasic firing type Is MNs in each hemisegment, which, based on the muscle groups they each innervate, are also known as ventral common exciter (vCE) and dorsal common exciter (dCE) MNs (44). Here, we sought to understand how the different MNs and muscles contribute to rolling.

We initially used *UAS-Kir2.1-eGFP* [an inwardly rectifying potassium channel (45)] to chronically silence different subsets of

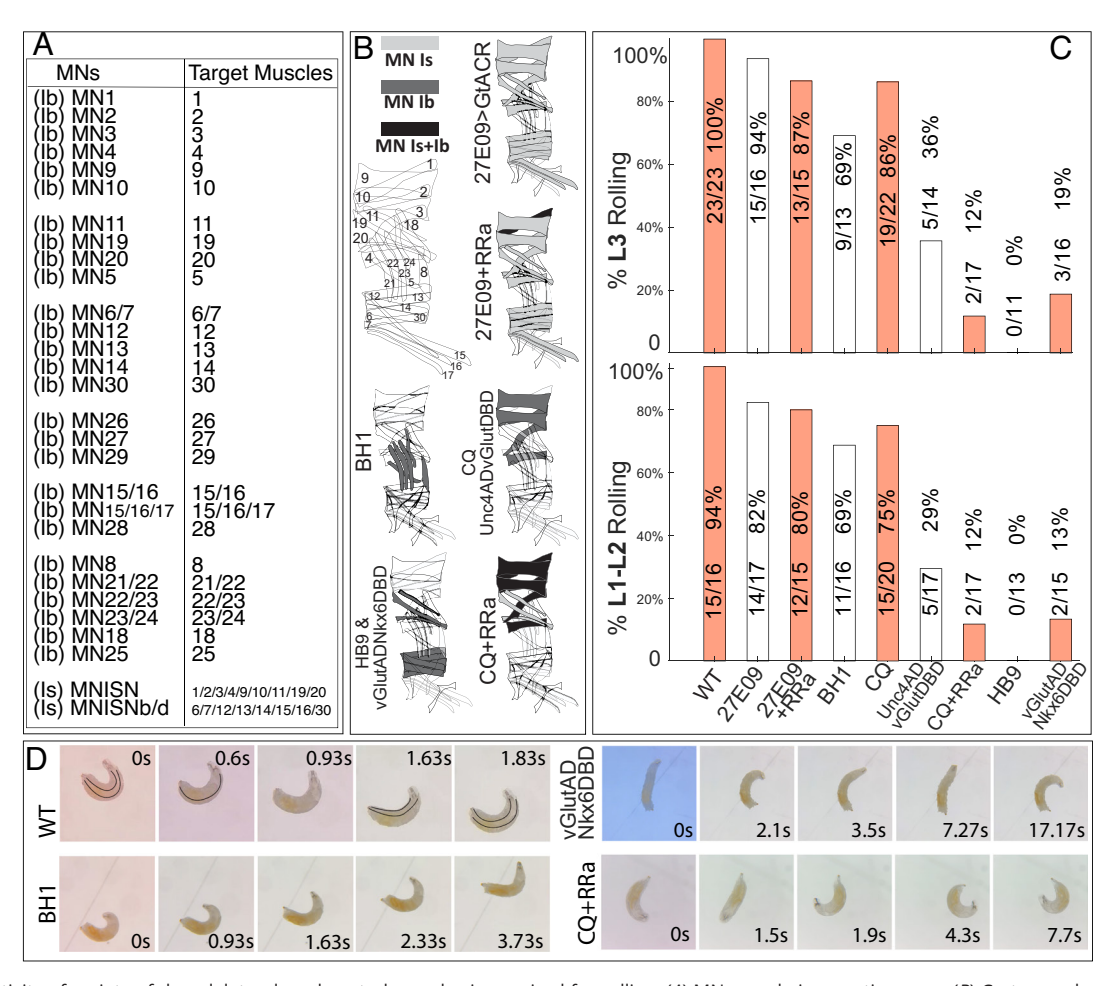


Fig. 4. The activity of variety of dorsal, lateral, and ventral muscles is required for rolling. (A) MN-muscle innervation map. (B) Cartoons showing the muscle groups in each genotype whose MN type Is (light gray), Ib (dark gray) or both Ib and Is (black) inputs are silenced. (C) Bar graphs showing the % of L3 (*Top* panel) and L1–L2 (*Bottom* panel) animals of different genotypes that are able to complete at least one complete roll. Silencing MN Is (*R27E09-UAS-GtACR1-eGFP*) or in combination with Ib MN1 (*R27E09+RRa>UAS-GtACR1-eGFP*) had little or no effect on rolling performance. Silencing Ib MNs of LT muscles (*BH1>UAS-GtACR1-eGFP*) leads to a slightly reduced chance of successful rolling. Silencing Ib MN of DL muscles caused mild (*CQ>UAS-GtACR1-eGFP*) to moderate (*Unc4^{AD}-vGlut^{DBD}>UAS-GtACR1-eGFP*) defect to rolling; however, silencing both Ib and Is targeting DL muscles (*CQ+RRa>UAS-GtACR1-eGFP*) lead to severe rolling failure. Silencing Ib MNs of VL and DO muscles (HB9>UAS-GtACR1-eGFP and *vGlut^{AD}-Nkx6^{DBD}>UAS-GtACR1-eGFP*) leads to near-complete failure in rolling. Control animals are *69E06-LexA>Aop-Chrimson-tdTomato*, *UAS-GtACR1-eGFP* while each MN silencing group also carries one or two *MN-Gal4* or *MN-split-Gal4* components. (*D*) Still images showing wild-type (*GORO>Chrimson*) rolling, and rolling in *BH1>UAS-GtACR1-eGFP*, *vGlut^{AD}-Nkx6^{DBD}>UAS-GtACR1-eGFP* and *CQ+RRa>UAS-GtACR1-eGFP* animals. Wild-type rolling is initiated by bending to one lateral side while the dorsal plane is facing upward (identified by both tracheae being visible, labeled with black lines), followed by continuous body rotation (still images showing 0°, 90°, 180°, 270° and 360° of an outward roll). A successful roll is defined as the completion of at least one 360° roll. A BH1>GtACR (LT Ib MN silencing) animal that can roll albeit at a slightly slower speed. *vGlut^{AD}-Nkx6^{DBD}-UAS-GtACR1-eGFP* (VL and DO Ib MN silencing) animals cannot bend their bodies enough to start rolling. *CQ+RRa>UAS-GtACR1-eGFP* (dorsal

MNs, while activating Goro command neurons with Chrimson to induce rolling. However, several control experiments led us to question the efficacy of UAS-Kir2.1-eGFP in silencing MNs (SI Appendix and Movie S7). Therefore, we tested the role of different MNs in rolling by optogenetically activating Goro command neurons with Goro-LexA>lexAop-Chrimson, and acutely silencing subsets of MNs using Gal4-driven GtACR1-GFP, an optogenetically activated chloride channel (Fig. 4B) (46). SI Appendix, Fig. S6 shows the CNS expression patterns of different MN-Gal4 lines used to drive UAS-GtACR1-eGFP. Our dual optogenetic approach allowed us to selectively silence the targeted MNs only during the time window when Goro-LexA>lexAop-Chrimson was activated by light, as GtACR1 opens and hyperpolarizes neurons in response to illumination. We used R27E09-Gal4 to exclusively express UAS-GtACR1-eGFP in type Is MNs and found that silencing of these common exciter MNs had no effect on larval rolling. In contrast, optogenetic silencing of type Ib MNs innervating the ventral longitudinal (VL) and dorsal oblique (DO) muscles using HB9-Gal4>UAS-GtACR1-eGFP eliminated both bending and rolling in L1/L2 and L3 animals (Fig. 4 C and D and Movie S8). Given the possible off-target expression of HB9-Gal4 in other neurons, we repeated this experiment using a recently developed split Gal4 line (vGlutAD-Nkx6DBD) (47) that specifically targets the same MNs (i.e., VL/DO MNs) as HB9-Gal4 and observed similar severe rolling and bending defects in L1/L2 and L3 animals (Fig. 4 C and D and Movie S8). Next, we used CQ-Gal4>UAS-GtACR1-eGFP to selectively silence five type Ib MNs innervating the dorsal longitudinal (DL) muscles and found that acute silencing of tonic inputs to DL muscles led to mild rolling defects, where 25% of L1 and 13% of L3 larvae failed to execute at least one complete 360° roll (Fig. 4 C and D and Movie S8). Since CQ-Gal4 has been reported to have a few off-targets (48), we repeated the DL silencing experiment using Unc4^{AD}-vGlut^{DBD}-Gal4 (49) to specifically express GtACR1-eGFP in the same MNs targeted by CQ-Gal4 line. $Unc4^{AD}$ - $vGlut^{DBD}$ >UAS-GtACR1-eGFP animals showed 68% and 42% rolling defects in L1/L2 and L3 stages, respectively, which is more severe than what we saw with CQ-Gal4 (Fig. 4 C and D and Movie S8). Taken together, the MN silencing data using $Unc4^{AD}$ - $vGlut^{DBD}$ and CQ-Gal4 lines demonstrate that tonic-firing type Ib MNs innervating DL muscles 2, 3, 4, 9, and 10 are important for larval rolling. In both *CQ-Gal4>UAS-GtACR1* and *Unc4*^{AD}-*vGlut*^{DBD}>*UAS-GtACR1-eGFP* animals, DL muscles 2, 3, 4, 9, and 10 still receive phasic excitatory inputs from the type Is MN (dCE) and the DL muscle 1 receives both Ib and Is inputs (Fig. 4 C and D and Movie S8). The ability of some CQ-Gal4> UAS-GtACR1-eGFP and Unc4^{AD}-vGlut^{DBD}>UAS-GtACR1-eGFP animals to perform complete rolls indicates that when Ib inputs to DL muscles 2, 3, 4, 9, and 10 are blocked, the phasic Is inputs to these muscles, along with the Ib and Is inputs to DL muscle 1, may be sufficient to fully or partially contract the dorsal area of the body wall during larval rolling, thereby preventing any disruption in the circumferential progression of muscle activity required to complete the roll. Therefore, to fully determine the role of DL muscles 1, 2, 3, 4, 9, and 10 in larval rolling, we used the CQ-Gal4+RRa-Gal4 line to silence both Ib (tonic) and Is (phasic) inputs to these muscles. In CQ-Gal4+RRa-Gal4>UAS-GtACR1-eGFP larvae, we observed 88% rolling defect in both L1/L2 and L3 animals, which is significantly higher than the defect seen in CQ-Gal4+RRa-Gal4>UAS-GtACR1-eGFP or CQ-Gal4>UAS-GtACR1-eGFP larvae (Fig. 4 C and D and Movies S8 and S9). Notably, CQ-Gal4+RRa-Gal4> UAS-GtACR1-eGFP animals could bend and initiate the roll; however, they could not execute a complete 360° rolling, corroborating that, as suggested in our biomechanical model for rolling (Fig. 3), the contraction of DL muscles and the resultant force imbalance are necessary for the larvae to complete the rolling already initiated due

to contraction of VL and LT muscles. Finally, we found that silencing Ib MN inputs to lateral transverse muscles (LTs) using BH1-Gal4>UAS-GtACR1-eGFP led to a 31% rolling defect, indicating that LTs are in part necessary for rolling behaviors. Given that the LT muscles do not seem to receive any phasic inputs from Is MNs (dCE and vCE), we did not examine larval rolling in 27E09-Gal4+BH1-Gal4>UAS-GtACR1-eGFP.

To determine the efficiency and specificity of GtACR1-eGFP driven by the Gal4 lines used in this study, in addition to confirming GFP expression in isolated larval brains (SI Appendix, Fig. S6), we performed muscle calcium imaging in intact larvae crawling forward under a confocal microscope. We found that GtACR1-eGFP driven by $vGlut^{AD}$ - $Nkx6^{DBD}$, HB9-Gal4, BH1-Gal4, R27E09-Gal4 + $Unc4^{AD}$ - $vGlut^{BD}$, and CQ-Gal4 lines effectively. tively blocked the activity of the desired MNs, as evidenced by almost complete lack of activity in their target muscles while the larvae performed forward crawling (SI Appendix, Fig. S7 and Movie S10). In contrast, we did not observe diminished GCaMP6f activity in any off-target muscles, indicating the specificity of these Gal4 lines. Taken together, we conclude that, consistent with our biomechanical model, ventral muscles are essential for initial bending, and muscles located in different dorsoventral regions of the larval body contribute to completion of the 360° roll. Furthermore, type Is MNs inputs may act in synergy with type Ib inputs to generate robust rolling behavior and partially compensate for the loss of Ib inputs; while in the absence of Is inputs, type Ib MNs can still drive robust rolls.

Identifying Candidate Circuits for Circumferential Muscle Contraction Sequences. We examined the electron microscopic (EM) connectome data (21, 50) to look for PMN–MN circuits that could support circumferential propagation of contraction. First, we identified multiple PMNs that synapse onto MNs with spatially clustered target muscles in the periphery. Specifically, PMNs that synapse primarily to MNs innervating one spatial muscle group are more likely to synapse onto neighboring regions around the circumference of the larva, such as dorsolateral muscles (i.e., DLs, DOs, and LTs), ventrolateral muscles (i.e., VOs, VLs, and LTs) (Fig. 5A and SI Appendix, Fig. S9A), and/or muscles flanking dorsal midline (i.e., left–right DLs) (Fig. 5B and SI Appendix, Fig. S9B). To verify this phenomenon across all PMNs, we observed the cosine similarity between individual PMN projection patterns relative to downstream muscle drive and found that muscles more proximal along the circumference of the larva have higher overlap in PMN drive than those distal to each other (SI Appendix, Fig. S9C). On the other hand, MNs that innervate spatially distant muscles (i.e., lateral transverse muscles LTs on the left and right side) receive inputs from an exclusive set of PMNs (i.e., right PMNs synapsing with right LTs and vice versa) (Fig. 5C and SI Appendix, Fig. S9B).

As a specific example for PMNs driving neighboring muscles, we found that two presumptive excitatory PMNs in the right hemisegment (A03a1_a1r and A03a3_a1r PMNs) are presynaptic to MNs innervating dorsolateral muscles (DLs and DOs) on the animal's right side, while they also make a smaller number of synapses with MNs innervating DL muscles on the left side (Fig. 5*D*). Thus, activity of these right A03 PMNs should strongly activate the right dorsolateral muscles and weakly activate the DL muscles on the left side. Then, activation of the left counterparts of these PMNs should have a mirror effect and strongly activate the left dorsolateral muscles while weakly activating the DL muscles on the right side. Sequential activation patterns of left and right A03 PMNs should therefore facilitate the circumferential progression of dorsolateral muscle contractions from right to left hemisegments, a pattern that is seen during clockwise rolling (Fig. 5E). Further analysis of

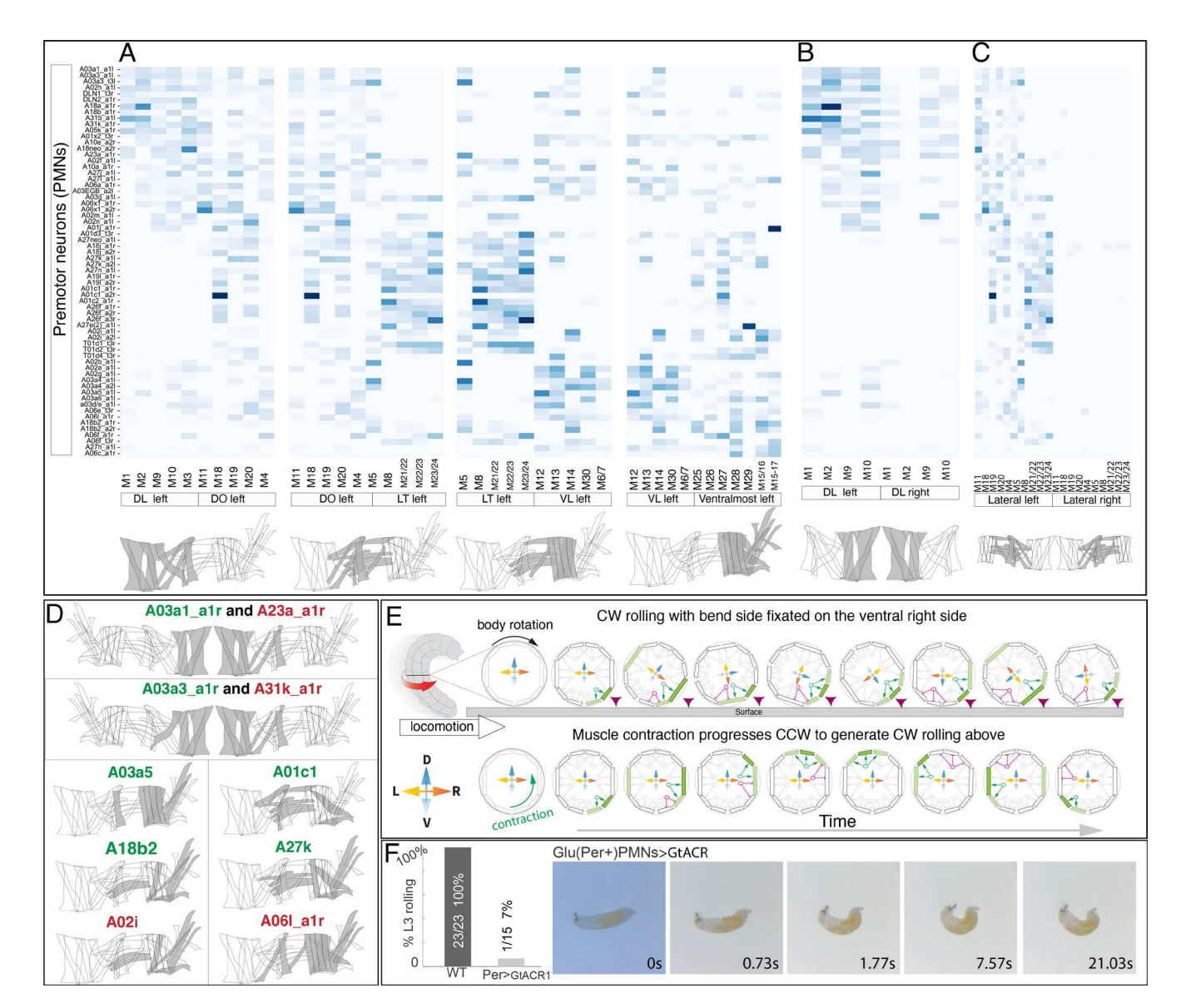


Fig. 5. Premotor circuit organization for circumferential progression of muscle activity observed during escape. (A-C) Heat maps representing the normalized weighted-synaptic output (blue shading) of left PMN (rows) onto different subsets of left MNs (columns). Grayed sketches at the bottom of heatmaps indicate the target muscles of MNs in heatmap. (A) PMNs demonstrate connectivity patterns with dorsoventral organization, where PMNs presynaptic to DL MNs also establish synapses with MNs innervating the neighboring DO muscles (Left), PMNs presynaptic to dorsolateral MNs also establish synapses with MNs innervating the neighboring lateral muscles (second from left), PMNs presynaptic to lateral MNs also establish synapses with MNs innervating the neighboring ventral muscles (second from right), and PMNs presynaptic to ventral MNs also establish synapses with MNs innervating the neighboring ventralmost muscles (Right). (B) Left PMNs presynaptic to left DL MNs also establish a significant number of synapses with right DL MNs. Left and right DL muscles span neighboring regions along the dorsal body midline. (C) Left PMNs presynaptic to left lateral/dorsolateral MNs have negligible connectivity with right DL MNs. Lateral/dorsolateral on the left and right sides are spatially distant from each other. (D) Individual PMNs tend to synapse with MNs that correlate with spatially proximal muscles. The target muscles of PMN-MN-muscle motifs are shown in gray. Excitatory and inhibitory PMNs are shown in green and red, respectively. (E) Schematic model showing that to generate clockwise rolling (Top panel), muscle contraction progresses counterclockwise (Low panel). Circles are cross-section depictions of a larva at different time points. Rectangular shapes around the circumference indicate the body wall muscles. Dark and light green indicate the fully and partially contracted muscles, respectively. Purple arrowheads indicate the fixated bend sides in the top panel. The dorsoventral axis rotates clockwise in the top panel, while it is fixated at the bottom panel. The green and magenta oval shapes indicate the excitatory and inhibitory inputs from active PMNs, respectively. Gray oval shapes indicate inactive PMNs. (F) Silencing A02-PMNs with per>GtACR-eGFP (51) leads to 93% rolling defects. Image credit: Reprinted from ref. 21, which is licensed under CC BY 4.0.

connectome data revealed that two inhibitory PMNs (A23a and A31k) have connectivity patterns similar to the excitatory A03a1 and A03a3 PMNs (Fig. 5*D*). Such a synaptic organization raises the possibility that circumferential propagation of MN activity could be followed by circumferential inhibition of muscles. As A23a and A31k inhibit dorsolateral muscles, other excitatory PMNs may activate lateral and/or ventrolateral muscles, thereby enforcing wave progression (Fig. 5*E*). Consistent with this model, we identified excitatory (e.g., A03a5, A01c1, A18b2, and A27k) and inhibitory PMNs (e.g., A02i and A06l) that synapse with MNs projecting to

muscles positioned in the lateral, ventrolateral, and ventral regions of the body wall (Fig. 5*D*).

To quantitatively test the significance of the observed circumferential structure of PMN–MN–muscle connections, we compared the dorsoventral structure of PMN–MN outputs to that which would be expected by chance. Specifically, we performed a shuffling procedure that preserves the general statistics of PMN–MN connectivity while randomizing specific PMN–MN pairs (*SI Appendix*, Fig. S9 *D* and *E*). We found that the dorsoventral structure of real PMN–MN–muscle connectivity patterns of all PMNs combined,

as well as only PMNs previously identified as excitatory or inhibitory, is significantly greater than expected by chance (SI Appendix, Fig. S9F). This supports the likelihood that multiple specific premotor motifs could aide in driving a circumferential wave of muscle contractions, like those detailed above, and with precisely timed handoff from excitatory to inhibitory PMNs (Fig. 5D). Taken together, the PMN-MN-muscle connectome is structured in a way that sequential firing of excitatory and then inhibitory PMNs in one side followed by the activation of their counterparts on the other side could underlie the progression of muscle contraction waves around the circumference of the larva (Fig. 5E).

There are multiple glutamatergic inhibitory A02-PMNs that have been implicated in larval crawling and rolling (27, 30, 51, 52). Based on the PMN-MN-muscle connectome dataset, each A02-PMN establishes synapses with MNs innervating nearby muscles that together span the entire dorsoventral axis of the larval body wall (SI Appendix, Fig. S10). We found that optogenetic silencing of A02-PMNs using per-Gal4 (51) led to severe rolling defects (Fig. 5F and Movie S11). In addition to PMNs, per-Gal4 may target other glutamatergic interneurons. Therefore, it will be intriguing to determine the role of individual or smaller subsets of A02-PMNs and other excitatory and inhibitory PMNs in generating rolling behavior.

Discussion

Escape is a fundamental form of locomotion and critical for the survival of all animals. To understand the neural mechanisms of an escape behavior, we have performed live imaging of muscle activity across animals as they perform rolling escape behavior, proposed models explaining the biomechanics of inward and outward rolls, analyzed a connectome for motor circuits that could support the unique muscle propagation wave that coordinates this escape motor program, and performed MN silencing experiments to determine muscle groups whose activity is necessary for rolling behavior. This work has illuminated fundamental distinctions and similarities between motor patterns underlying forward crawling and escape in the larva and starts to uncover the circuit basis for rolling escape motor response.

Enhancements of SCAPE Microscopy to Permit Studies of Rolling Behavior. Our ability to identify patterns of muscle activity during rolling was aided by the further development of dual-color SCAPE. SCAPE microscopy has previously captured muscles in behaving larvae (31) and dual-color proprioceptor activity during crawling behavior (33). Resolution and field of view were improved in the version of dual-color SCAPE imaging used here, enabling ratiometric quantification of muscle activity and discrimination of activity signals from passive changes in fluorophore density within muscles. This imaging method also allowed measurement across muscles at different focal depths during freely moving behavior, including muscles within the C-shaped bend during rolling escape behavior. Further expanding SCAPE's field of view, or implementing a system that can view larvae from multiple viewpoints could allow simultaneous imaging in the CNS and muscles and test some of the hypotheses about PMN to MN transformations that underlie rolling, and a number of other behaviors, in simple model organisms.

Separable Sequences of Muscle Activity during Rolling. Animal movement universally involves coordinated sequential muscle activity. We find that the segmentally synchronous circumferential progression of muscle contractions define escape rolling behavior in Drosophila larvae. This sequence of activity progresses in a clockwise or counterclockwise manner, which determines the direction of rolling. A recent independent investigation similarly found that a circumferential wave of muscle activity occurs during rolling (53). Whether the circumferential sequence is the primary motor activity that promotes rolling, or whether other independent patterns are involved, is so far unclear. However, our muscle imaging revealed evidence that, during rolling, LT and VA muscles contract as part of a separate, out-of-phase sequence relative to the major wave of activity of longitudinal muscles. LT muscles begin to contract after D and V longitudinal muscles also during crawling (21, 50, 52), suggesting special roles for these muscles in both forms of locomotion. During forward crawling, contraction of LT muscles shortens the dorsoventral axis, providing a force that is thought to push the neighboring internal organs to the anterior side (20). We propose that during rolling, sustained LT and VA muscle activity ensures the optimal rigidity necessary for the larval soft body to function as a muscular hydrostat, which is reminiscent of the structural rigidity required for function of boneless hydrostatic skeletons, such as animal tongues and cephalopod arms (41). Interestingly, while silencing the LT-innervating MNs substantially compromises rolling behavior, it does not seem to perturb the execution of forward peristalsis itself (27), but reduces the peristalsis frequency and thereby crawling speed (54).

One crucial future goal will be to understand how segmentally synchronous contractions of specific groups of muscles are initiated and then how contraction propagates to other muscle groups in a precise circumferential sequence during rolling. The fundamental distinctions between bodily coordination during rolling versus crawling illustrate the remarkable propensity for even relatively simple nervous systems to generate vastly different circuit dynamics based on context. Prior to this work, it was unknown whether rolling escape would involve a peristaltic wave component, like that observed in crawling, and our work argues against a peristaltic component to rolling. Understanding at a circuit level how the larval motor system switches between these two patterns of activity remains an important future goal. It will be especially important to determine whether excitatory and inhibitory microcircuit motifs that coordinate crawling (43, 55) also coordinate rolling muscle contractions. Further, understanding how the larva transitions between peristaltic and rolling escape locomotor modes remains an open question.

Laws of Mechanics Underlying Larval Rolling Escape Behavior.

We present biomechanical models aiming to explain how counterclockwise circumferentially progressing muscular contraction generates clockwise rolling motion and vice versa. In our proposed models, the rolling behavior emerges as a stabilizing response generated via instantaneous torque (i.e., moment) imbalance owing to the offset of the ground reaction forces and weight offset induced by bending. In a larva lying flat on a surface with no bending, the center of gravity (CoG) is located at the central axis of the body and the weight nullifies the ground reaction forces. For our rolling biomechanical model to work, the larva must bend to either side to assume an arc shape, causing the CoG to move away from the central axis. We expect that for the most efficient rolling escape maneuver, there should be an optimal arc shape, and the larval body with either of the two extreme shapes, straight or circular, would fail to produce translation on the surface (i.e., movement) because of its inability to produce a net friction force due to the coinciding weight and ground reaction forces. A segmentally repeated pair of interneurons, known as down and back (DnB), has been shown to play a key role in bending and rolling (30). Animals with silenced DnB neurons can perform rolling but with a significantly reduced rolling frequency. Importantly, silencing DnB neurons dramatically decreased the curvature of the C-shaped bending (30). It will be intriguing to determine whether the reduced curvature resulting from DnB silencing compromises the distance that the

larva travels (translates) per roll. Since DnBs receive inputs from sensory neurons responding to noxious and tactile stimuli, it will be interesting to determine whether there is any correlation between the level of noxious input, curvature of the C bend, and the translation distance traveled per roll. Optogenetically activating nociceptive neurons with different intensities of light could be a possible way to regulate the intensity of the noxious insult. DnB neurons are cholinergic excitatory neurons that provide direct synaptic input to multiple excitatory and inhibitory premotor neurons. Selective silencing of these premotor neurons will be an important future direction aimed at understanding how the coordinated activity of different groups of excitatory and inhibitory premotor neurons results in the optimal curvature and circumferential propagating muscular activity essential for roll generation.

Insights into Motor Circuits Critical for Rolling Behavior. Our functional manipulations of MNs innervating distinct muscle subgroups highlight the modularity of motor control in larval rolling escape behavior. Larvae can exclusively bend or perform bending and rolling. Our MN silencing experiments demonstrate that longitudinally spanning ventral muscles are essential for larval bending and rolling altogether, while longitudinally spanning dorsal muscles and lateral transverse muscles are only essential for completion of rolling. These findings are congruent with previous work demonstrating that neurons driving transverse muscles are essential for body rotation in self-righting (56) and rolling (27).

The relative roles of Is and Ib MNs in different larval behaviors are still debated (42, 57-59). Our MN silencing experiments showed that silencing type Ib MNs led to more severe rolling defects in rolling behavior than when the broadly projecting type Is MNs were silenced. Furthermore, the simultaneous silencing of Ib and Is MNs led to more severe rolling defects than when only Ib MNs were silenced, suggesting that phasic Is inputs may partially compensate for the loss of tonic Ib inputs. Phasic Is MNs have a higher probability of vesicle release at the NMJ, demonstrate elevated presynaptic calcium influxes upon stimulation, and contain larger synaptic vesicles per synapse than tonic Ib MNs, leading to higher amplitude EPSPs in muscles following type Is activity (57, 60, 61). For these reasons, Ib and Is MNs are sometimes called "weak" and "strong" MNs, respectively (57, 60). On the other hand, type Ib NMJs have higher levels of readily releasable vesicle pool, a higher number of active release sites than Is boutons, and are recruited earlier and for a longer duration during larval movement (57-60). These physiological properties of type Ib tonic and type Is phasic MNs are determined by their distinct transcriptional profiles (61), and permit a division of labor during muscle contraction, where type Ib activity can coordinate specific, finer muscle contraction timing with varying levels of contractile force upon low-level premotor input, while type Is activity is recruited at high-level premotor input to increase contractile force of ongoing behavior or make large, forceful shifts in movement (57-60). In conjunction with our results, these properties suggest that type Ib MNs are crucial for driving the main muscle contraction pattern underlying rolling, while type Is MNs merely contribute additional contractile force to rolling, consistent with the minimal impact of type Is MN silencing on crawling behavior (58). These findings are also consistent with tonic and phasic motor control principles observed in mammalian systems (62-64), adult Drosophila walking (65) and flight (66), and other escape motor circuits (18).

We uncovered patterns of PMN–MN connectivity that could support propagation of muscle contractions around the circumference of the larva during rolling behavior. Studies of PMNs that innervate midline muscles could reveal how the circumferential wave progresses from left to right sides of the larva's body. Bridging

the gap between Goro escape-promoting command neurons to specific excitatory and inhibitory PMNs through further connectome reconstruction and circuit manipulation is a crucial next step in understanding the basis of larval rolling escape behavior. Continued pursuit of the sensorimotor circuits that drive escape in the larva will more broadly uncover the circuit mechanisms responsible for transforming sensory information into robust and flexible behaviors across taxa.

Materials and Methods

SCAPE Image Acquisition. A custom-built Swept Confocally Aligned Planar Excitation (SCAPE) microscope, extended from that described in Voleti et al. (35) and Vaadia et al. (33), was used to acquire high-speed volumetric imaging of rolling larvae. See SI Appendix for SCAPE image acquisition, processing, and analysis.

Neural Silencing Combined with Rolling Assays. 69E06-LexA; Aop-ChrimsontdTomato, UAS-GtACR1-eGFP flies were crossed with MN-Gal4 or w 1118 lines for experimental and control groups, respectively. For all crosses involving MN silencing with GtACR1-eGFP, L1, L2, and L3 larvae of the experimental and control groups were used. Rolling success was defined as a larva completing at least one 360° roll (after body bending, able to rotate in a single direction from dorsal side up to dorsal side up). See SI Appendix for more experimental details.

Quantitative Analysis of the PMN-MN Connectome. The raw data (connectivity matrix, PMN-MN connectome, and xyz coordinates of MN post synapses) originally used to generate figures 5 and 7 published in Zarin et al. (21) were reused with permission from eLife Sciences Publications, Ltd. These raw data were used to make current Fig. 5 and *SI Appendix*, Figs. S8–S10 of this paper. See SI Appendix for more details.

Data, Materials, and Software Availability. Behavioral analysis, 3D averaging, signal extraction, and subsequent muscle activity analysis were performed using custom MATLAB scripts that have been included with manuscript submission and are also available here: https://github.com/cooneypc4/larval_escape_manuscript (67). Larva 3D model and animation were generated with Blender 3.3.9 (Blender Foundation). Figures and supplementary videos are assembled with Adobe Illustrator 2023 and Adobe Premiere Pro 2023 (Adobe).

ACKNOWLEDGMENTS. We thank Ashok Litwin-Kumar for providing guidance on quantitative analysis of connectome data. We thank Albert Cardona, Richard D. Fetter, and the HHMI Janelia Fly EM Project Team for providing the raw data of the whole CNS EM volume. We thank Akira Fushiki and Maarten Zwart for annotating neurons, and Keiko Hirono for generating transgenic constructs. We thank Grace Shin for assisting with behavioral assay development. We thank Malte Casper for supporting SCAPE data processing and Citlali Perez Campos and Richard Wenwei Yan for contributions to SCAPE hardware development. Stocks obtained from the Bloomington Drosophila Stock Center (NIH P400D018537) were used in this study. Research reported in this publication was supported by an institutional startup fund from Texas A&M University (A.A.Z.), NIH NINDS R01NS061908 (W.B.G), NIH BRAIN 5U01NS094296 and 1UF1NS108213 (E.M.C.H.), DoD, MURI W911NF-12-1-0594, and Simons Foundation Collaboration on the Global Brain (E.M.C.H.), the NSF Grants IIS-2008797 and CMMI-2048142 (I.S.G), and an NSF predoctoral fellowship DGE 2036197 (P.C.C.). The content is solely the responsibility of the authors and does not necessarily represent the official views of the NIH.

Author affiliations: ^aGrueber Laboratory, Mortimer B. Zuckerman Mind Brain Behavior Institute, Columbia University, New York, NY 10027; ^bDepartment of Neuroscience, Institute, Columbia University, New York, NY 10027; Department of Biology, Texas A&M University, College Station, TX 77843; Grain Laboratory, Texas A&M Institute for Neuroscience, Texas A&M University, College Station, TX 77843; Laboratory for Functional Optical Imaging, Mortimer B. Zuckerman Mind Brain Behavior Institute, Columbia University, New York, NY 10027; Department of Electrical Engineering, Columbia University, New York, NY 10027; ^gDepartment of Multidisciplinary Engineering, Texas A&M University, College Station, TX 77843; hDepartment of Engineering Technology and Industrial Distribution, Texas A&M University, College Station, TX 77843; ¹J. Mike Walker '66 Department of Mechanical Engineering, Texas A&M University, College Station, TX 77843; ¹Department of Biomedical Engineering, Columbia University, New York, NY 10027; ¹Laboratory for Functional Optical Imaging, Kavli Institute for Brain Science, Columbia University, New York, NY 10032; and ¹Department of Physiology and Cellular Biophysics, Jerome L. Greene Science Center, New York, NY 10037 New York, NY 10027

- D. Arendt, M. A. Tosches, H. Marlow, From nerve net to nerve ring, nerve cord and brain-evolution of the nervous system. Nat. Rev. Neurosci. 17, 61-72 (2016).
- T. Branco, P. Redgrave, The neural basis of escape behavior in vertebrates. Ann. Rev. Neurosci. 43,
- G. M. Card, Escape behaviors in insects. Curr. Opin. Neurobiol. 22, 180-186 (2012).
- M. Dickinson, C. F. Moss, Neuroethology. Curr. Opin. Neurobiol. 22, 177-179 (2012).
- P. Domenici, J. M. Blagburn, J. P. Bacon, Animal escapology. I: Theoretical issues and emerging trends in escape trajectories. J. Exp. Biol. 214, 2463-2473 (2011).
- P. Domenici, J. M. Blagburn, J. P. Bacon, Animal escapology. II: Escape trajectory case studies. *J. Exp.* Biol. 214, 2474-2494 (2011).
- O. D. Broekmans et al., Resolving coiled shapes reveals new reorientation behaviors in C. elegans. eLife 5, 1-17 (2016).
- D. H. Edwards et al., Fifty years of a command neuron-The neurobiology of escape behavior in the crayfish. Trends Neurosci. 22, 153-161 (1999).
- R. C. Eaton, R. K. K. Lee, M. B. Foreman, The Mauthner cell and other identified neurons of the brainstem escape network of fish. Prog. Neurobiol. 63, 467-485 (2001).
- T.-C. Huang, Y.-J. Huang, W.-C. Lin, Real-time horse gait synthesis. Comput. Animation Virtual Worlds 24, 87-95 (2013).
- O. Kiehn, Decoding the organization of spinal circuits that control locomotion. Nat. Rev. Neurosci. 17, 224-238 (2016).
- H. Fotowat, R. R. Harrison, F. Gabbiani, Multiplexing of motor information in the discharge of a 12. collision detecting neuron during escape behaviors. Neuron 69, 147-158 (2011).
- J. M. Hemmi, D. Tomsic, The neuroethology of escape in crabs: From sensory ecology to neurons and 13. back. Curr. Opin. Neurobiol. 22, 194-200 (2012).
- ${\sf C.\,R.\,von\,Reyn}\,\textit{et\,al.,}\, {\sf Feature\,integration\,drives\,probabilistic\,behavior\,in\,the\,Drosophila\,escape}$ 14. response. Neuron 94, 1190-1204.e6 (2017).
- J. M. Ache et al., Neural basis for looming size and velocity encoding in the Drosophila giant fiber 15. escape pathway. Curr. Biol. 29, 1073-1081.e4 (2019).
- 16. T. W. Dunn et al., Neural circuits underlying visually evoked escapes in larval zebrafish. Neuron 89, 613-628 (2016).
- J. L. Donnelly et al., Monoaminergic orchestration of motor programs in a complex C. elegans behavior. PLoS Biol. 11, e1001529 (2013).
- D. Kennedy, K. Takeda, Reflex control of abdominal flexor muscles in the crayfish. J. Exp. Biol. 43,
- M. Bate, The embryonic development of larval muscles in Drosophila. Development 110, 791-804
- E. S. Heckscher, S. R. Lockery, C. Q. Doe, Characterization of Drosophila larval crawling at the level of 20.
- organism, segment, and somatic body wall musculature. J. Neurosci. 32, 12460-12471 (2012). A. A. Zarin et al., A multilayer circuit architecture for the generation of distinct locomotor behaviors in Drosophila. eLife 8, 1-34 (2019).
- 22. W. D. Tracey Jr. et al., painless, a Drosophila gene essential for nociception. Cell 113, 261-273 (2003).
- R. Y. Hwang et al., Nociceptive neurons protect Drosophila larvae from parasitoid wasps. Curr. Biol. 17, 2105-2116 (2007).
- J. L. Robertson, A. Tsubouchi, W. D. Tracey, Larval defense against attack from parasitoid wasps
- requires nociceptive neurons. PLoS ONE 8, e78704 (2013). W. B. Grueber, L. Y. Jan, Y. N. Jan, Dendritic tiling in Drosophila. Development 129, 2867–2878 (2002).
- T. Ohyama et al., A multilevel multimodal circuit enhances action selection in Drosophila. Nature **520**, 633-639 (2015).
- J. Yoshino et al., Neural circuitry that evokes escape behavior upon activation of nociceptive sensory neurons in Drosophila larvae. Curr. Biol. 27, 2499-2504.e3 (2017).
- C. Hu et al., Sensory integration and neuromodulatory feedback facilitate Drosophila mechanonociceptive behavior. Nat. Neurosci. 20, 1085-1095 (2017).
- S. Takagi et al., Divergent connectivity of homologous command-like neurons mediates
- segment-specific touch responses in Drosophila. *Neuron* **96**, 1373–1387.e6 (2017).

 A. Burgos *et al.*, Nociceptive interneurons control modular motor pathways to promote escape behavior in Drosophila. eLife 7, e26016 (2018).
- M. B. Bouchard et al., Swept confocally-aligned planar excitation (SCAPE) microscopy for high-speed
- volumetric imaging of behaving organisms. Nat. Photonics 9, 113-119 (2015). E. M. C. Hillman et al., High-speed 3D imaging of cellular activity in the brain using axially-extended
- beams and light sheets. Curr. Opin. Neurobiol. 50, 190-200 (2018). R. D. Vaadia et al., Characterization of proprioceptive system dynamics in behaving Drosophila
- larvae using high-speed volumetric microscopy. Curr. Biol. 29, 935-944.e4 (2019).
- E. M. C. Hillman et al., Light-sheet microscopy in neuroscience. Annu. Rev. Neurosci. 42, 295-313 (2019).
- V. Voleti et al., Real-time volumetric microscopy of in vivo dynamics and large-scale samples with SCAPE 2.0. Nat. Methods 16, 1054-1062 (2019).

- 36. L. Xu et al., Widespread receptor-driven modulation in peripheral olfactory coding. Science 368, eaaz5390 (2020)
- E. S. Schaffer et al., Flygenvectors: The spatial and temporal structure of neural activity across the fly brain. bioRxiv [Preprint] (2021). https://doi.org/10.1101/2021.09.25.461804 (Accessed 26 September 2021).
- S. E. Benezra et al., Learning enhances behaviorally relevant representations in apical dendrites. bioRxiv [Preprint] (2021). https://doi.org/10.1101/2021.11.10.468144 (Accessed 11 November 2021).
- D. K. Dimuthu et al., "Dynamic modeling and validation of soft robotic snake locomotion," in IEEE International Conference on Control, Automation and Robotics (ICCAR) (2023).
- 40. D. K. Dimuthu, Y. C. Arachchige, I. S. Godage, "Soft robotic snake locomotion: Modeling and experimental assessment," in IEEE 17th International Conference on Automation Science and Engineering (CASE) (2021).
- W. M. Kier, The diversity of hydrostatic skeletons. J. Exp. Biol. 215, 1247-57 (2012).
- S. Peron et al., From action potential to contraction: Neural control and excitation-contraction coupling in larval muscles of Drosophila. Comp. Biochem. Physiol. A, Mol. Integr. Physiol. 154, 173-183 (2009).
- M. Q. Clark et al., "Neural circuits driving larval locomotion in Drosophila" in Neural Development, J. A. Kaltschmidt, T. R. Clandinin, Eds. (BioMed Central Ltd., 2018).
- 44. Y. Wang et al., Structural and functional synaptic plasticity induced by convergent synapse loss in the Drosophila neuromuscular circuit. J. Neurosci. 41, 1401-1417 (2021).
- R. A. Baines et al., Altered electrical properties in Drosophila neurons developing without synaptic transmission. J. Neurosci. 21, 1523-1531 (2001).
- F. Mohammad et al., Optogenetic inhibition of behavior with anion channelrhodopsins. Nat. Methods **14**, 271-274 (2017).
- H. Lacin et al., Neurotransmitter identity is acquired in a lineage-restricted manner in the Drosophila CNS. eLife 8, e43701 (2019).
- A. Mauss et al., Midline signalling systems direct the formation of a neural map by dendritic targeting in the Drosophila motor system. PLoS Biol. 7, e1000200 (2009).
- H. Lacin et al., Unc-4 acts to promote neuronal identity and development of the take-off circuit in the Drosophila CNS. eLife 9, e55007 (2020).
- M. F. Zwart et al., Selective inhibition mediates the sequential recruitment of motor pools. Neuron 91, 615-628 (2016).
- H. Kohsaka et al., A group of segmental premotor interneurons regulates the speed of axial locomotion in Drosophila larvae. Curr. Biol. 24, 2632-2642 (2014).
- H. Kohsaka et al., Regulation of forward and backward locomotion through intersegmental feedback circuits in Drosophila larvae. Nat. Commun. 10, 2654 (2019).
- L. He, L. Borjon, W. Daniel TraceyJr., The motor pattern of rolling escape locomotion in Drosophila larvae. bioRxiv [Preprint] (2022). https://doi.org/10.1101/2022.11.03.514605 (Accessed 3 November 2022).
- $Y. \, Liu \, \textit{et al.}, Synchronous \, multi-segmental \, activity \, between \, metachronal \, waves \, controls \, locomotion \, activity \, between \, metachronal \, waves \, controls \, locomotion \, activity \, between \, metachronal \, waves \, controls \, locomotion \, activity \, between \, metachronal \, waves \, controls \, locomotion \, activity \, between \, metachronal \, waves \, controls \, locomotion \, activity \, between \, metachronal \, waves \, controls \, locomotion \, activity \, between \, metachronal \, waves \, controls \, locomotion \, activity \, between \, controls \, locomotion \, activity \, between \, controls \, locomotion \, activity \, between \, controls \, locomotion \, activity \, controls \, locomotion \, controls \, locomotion \, controls \, control$ speed in Drosophila larvae. eLife 12, e83328 (2023).
- I. Hunter et al., The Drosophila larval locomotor circuit provides a model to understand neural circuit development and function. Front. Neural Circ. 15, 684969 (2021).
- J. Picao-Osorio et al., MicroRNA-encoded behavior in Drosophila. Science 350, 815-820 (2015).
- K. He et al., Physiologic and nanoscale distinctions define glutamatergic synapses in tonic vs phasic neurons. J. Neurosci. 43, 4598-4611 (2023).
- Z. L. Newman et al., Input-specific plasticity and homeostasis at the Drosophila larval neuromuscular junction. Neuron 93, 1388-1404.e10 (2017).
- J. E. Schaefer, J. W. Worrell, R. B. Levine, Role of intrinsic properties in Drosophila motoneuron recruitment during fictive crawling. J. Neurophysiol. 104, 1257-1266 (2010).
- Y. Han et al., Botulinum neurotoxin accurately separates tonic vs. phasic transmission and reveals heterosynaptic plasticity rules in Drosophila. eLife 11, e77924 (2022).
- S. K. Jetti et al., Molecular logic of synaptic diversity between Drosophila tonic and phasic motoneurons. bioRxiv [Prerpint] (2023). https://doi.org/10.1101/2023.01.17.524447. E. Henneman, Relation between size of neurons and their susceptibility to discharge. *Science* **126**,
- 1345-1346 (1957).
- E. Henneman, G. Somjen, D. Carpenter, Functional significance of cell size in spinal motoneurons. J. Neurophysiol. 28, 560-580 (1964).
- E. Henneman, G. Somjen, A. David, Excitability and inhibitibility of motoneurons of different sizes. J. Neurophysiol. 28, 599-620 (1965).
- A. W. Azevedo et al., A size principle for recruitment of Drosophila leg motor neurons. eLife 9, 1-36 (2020).
- T. Lindsay, A. Sustar, M. Dickinson, The function and organization of the motor system controlling flight maneuvers in flies. Curr. Biol. 27, 345-358 (2017).
- P. Cooney, Larval_escape_manuscript. Github. https://github.com/cooneypc4/larval_escape_manuscript. Deposited 22 February 2023.